

Random focusing of sound into spatially coherent regions

J R Potter^{†‡}, B J Uscinski^{‡§} and T Akal^{||}

[†] Acoustic Research Laboratory, Tropical Marine Science Institute, National University of Singapore, 10 Kent Ridge Crescent, Singapore 119260

[‡] Department of Applied Mathematics and Theoretical Physics, Cambridge University, Cambridge, UK

[§] Applied Physics Laboratory and Department of Electrical Engineering, University of Washington, Seattle, WA 98015, USA

^{||} Saclantcen Undersea Research Centre, Viale San Bartolomeo 400, La Spezia 19026, Italy

E-mail: <http://www.arl.nus.edu.sg>

Received 25 August 1998, in final form 5 September 1999

Abstract. Oceanographic variability creates a weak random propagation medium for acoustic waves. The impact on acoustic transmission is becoming increasingly appreciated as the deterministic modelling of sound propagation in the ocean has become tractable and better understood. Beyond the near field (where phase fluctuations are weak) and the far field (where the scintillation index becomes saturated) multiple-scattering theory predicts that random focusing will greatly enhance the acoustic energy density over small volumetric regions, which we call 'ribbons'. In 1986 an experiment was carried out in the eastern Mediterranean to test this prediction using acoustic propagation along distinct, resolvable ray paths. This experiment is one of the few to map the spatial structure of acoustic intensity with such a large vertical aperture, and as far as the authors are aware it remains the only experiment to attempt to detect the two-dimensional structure of the predicted focused ribbons for individual energy paths. Renewed impetus to publish the results has been provided by the recent focus on moderate- to high-frequency acoustics in near-shore and shallow-water environments. The experiment is described and high-intensity regions consistent with the theoretical predictions are reported. A 3.5 kHz pulsed signal was transmitted over ranges of 11–23 km and sampled over a vertical aperture of 250–350 m and horizontal apertures of 4–4.5 km. The acoustic signals travelling along individual ray paths developed randomly focused regions of 6–18 dB over regions with a vertical dimension of about 20 m and whose horizontal length could possibly be up to 1 km. The understanding of these features allows system limitations to be estimated quantitatively and opens up the way to their constructive tactical use. The results are applicable to many systems from towed array sonars to high-frequency bathymetric sidescan and minehunting.

1. Introduction

This paper describes an experiment carried out jointly by the Saclant Undersea Research Centre and the Ocean Acoustics group of the Department of Applied Mathematics and Theoretical Physics, Cambridge University. The experiment was performed in the eastern Mediterranean to investigate the effect of sub-meso-scale ocean inhomogeneities on acoustic propagation. The objective was to investigate experimentally the possible existence of high-energy acoustic ribbons predicted by multiple-scattering theory. We emphasize that these randomly focused high-intensity regions are not in any way related to the familiar variations in intensity that arise from diffraction or coherent multiple-path interference, but are a result of random focusing of a single wavefront associated with a single identifiable ray path. An introduction to

the theoretical predictions is given first, followed by the background oceanography of the experimental site.

1.1. Theoretical background

The solution of the fourth-moment equation for a randomly and multiply scattered wave field has made the understanding of weak multiple-scattering effects on wave propagation more complete [1]. Specifically, it is now understood that there should exist a region between the near (unsaturated) and far (saturated) fields in which large variations in field intensity can occur. It is in this range where the most significant divergence occurs between the fourth-moment solution and the oft-used repeated Rytov scattering approximation. The most remarkable feature is the prediction of spatially coherent high-intensity ‘ribbons’ embedded in the medium. These are caused by the random phase modulations experienced by a wavefront propagating in a medium with a stochastically perturbed speed of sound. The modulations impart local curvatures to the wavefront which result in randomly focused regions further along the propagation path as phase modulations propagate into intensity modulations. The scattering inhomogeneities behave as a random many-segment lens system.

The two-point statistics of the field intensity in this region are known to be strongly non-Gaussian [2]. The distribution is skewed, so that intensity variations can often greatly exceed the RMS variability. This is of obvious interest to astronomers observing objects through interstellar gas and the Earth’s atmosphere (for whom the theory was originally developed) and more recently to underwater acousticians, who remain unable to explain some acoustic propagation variability with less complete approximations. Ewart [3] has complemented the (rather difficult) analytical results by fitting a generalized gamma distribution to describe the signal statistics of multiply weakly scattered acoustic propagation over a wide range of parameter space. The general characterization of these random phase and intensity fluctuations is of considerable importance. It not only permits improved sonar systems design but can serve as a remote sensing tool to probe current flow, inhomogeneity structure and turbulent dissipation as Farmer and his colleagues have shown (e.g. Farmer and Crawford [4], DiIorio and Farmer [5]).

However, it is in the intermediate range between the near and far field where the most interesting features are predicted, and where we seek to confirm the fourth-moment theory. Here, the intensities are predicted to be mostly smoothly varying and close to the expected estimated mean value, punctuated by occasional narrow regions of highly anomalous intensity values. These high-intensity ribbons are most clearly evident in the numerical simulations of wave propagation through a multiply scattering weakly random medium carried out by Macaskill and Ewart [6] and Uscinski [7]. These simulations were carried out in two dimensions, but similar features are seen in the three-dimensional simulations performed by Joia [8]. If one were to draw contour surfaces of the iso-intensity anomaly in three-dimensional space, these anomalous regions would appear as elongated flattened shapes, rather like deflated balloons. A sketch visualization of such a ribbon contour resulting from near-horizontal acoustic propagation in the ocean is given in figure 1. The three-dimensional ribbon is projected onto a vertical plane in the direction of propagation and another transverse to the propagation to illustrate the three spatial scales of the feature. Approximate expressions for the spatial dimensions (ζ , η , ξ) as functions of the vertical and horizontal scattering scales (L_v and L_h), scattering strength parameter (Γ), propagation range (x) and the characteristic ‘Fresnel’ range (x_0) have been employed following Uscinski [9]. The Fresnel range x_0 is a measure of the propagation distance required for phase modulations to fully

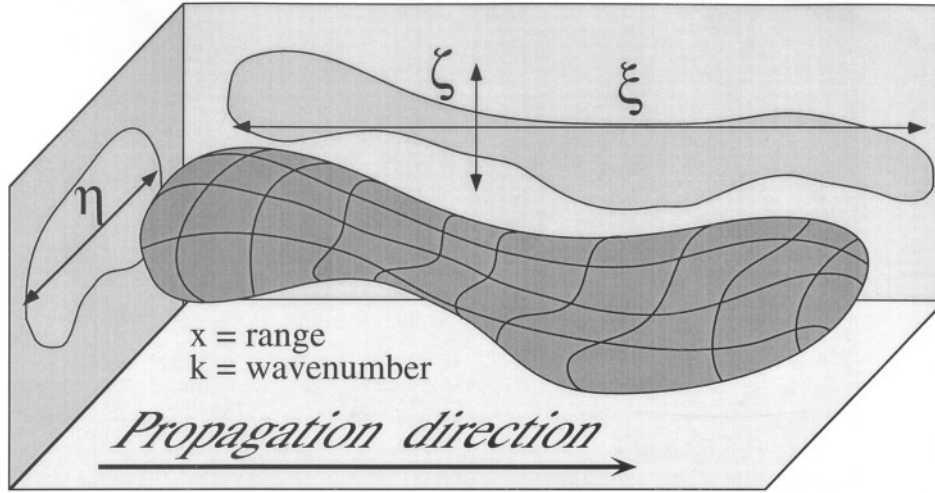


Figure 1. Visualization of an iso-anomaly contour for a high-intensity ribbon in the region of random focusing. L_h , horizontal variability scale; L_v , vertical variability scale; ‘Fresnel’ range, $x_0 = kL_v^2$; $\Gamma = k^3\mu^2L_hL_v^2$. $\eta \approx L_h(2\Gamma x/x_0)^{-1/2}$, $\zeta \approx L_v(2\Gamma x/x_0)^{-1/2}$, $\xi \approx x_0^2/(2\Gamma x)$.

develop into amplitude modulations and depends on L_v and k , the amplitude of the acoustic wavenumber.

The expressions all involve the scattering strength Γ , which is a naturally occurring parameter of multiple-scattering theory. The scattering strength parameter Γ is itself a function of L_v , L_h , k and the inhomogeneity strength (μ^2), defined as the variance of the fractional sound-speed variability. For multiply scattered waves, $\Gamma \geq O(10^2)$ and in the randomly focused region, where $x \leq O(x_0)$, the parameter $2\Gamma x/x_0 \geq O(10^1)$ so that $\zeta < L_v$ and $\eta < L_h$. This means that the characteristic ribbon width and height are each somewhat less than the respective sound-speed inhomogeneity characteristic scales in the horizontal and vertical directions. The ribbon length in the direction of propagation, ξ , is normally the largest dimension, so that the shape is shrunken and greatly elongated with respect to the propagation inhomogeneities.

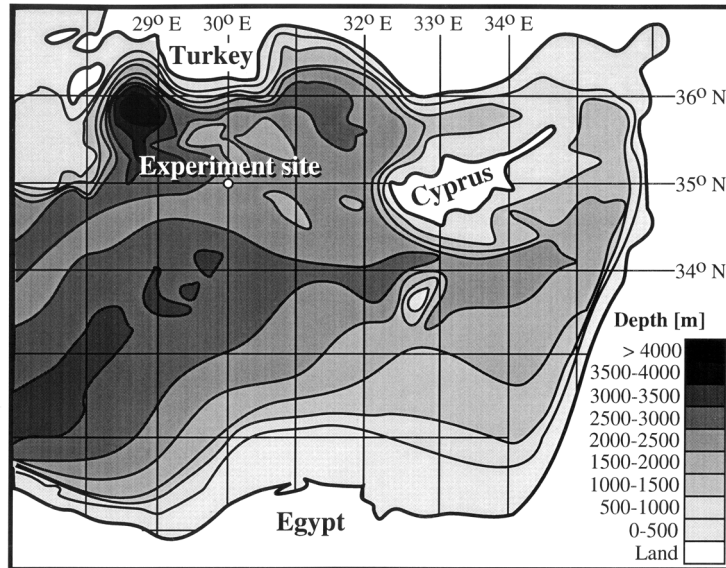
1.2. Ocean-acoustic background

The first question is whether the inhomogeneity scales for acoustic propagation in the ocean result in physically realizable scales for the ribbons. Approximate values for the space and time coherence scales of an acoustic ribbon can be evaluated at the characteristic focusing range $x_f = 0.9\Gamma^{-1/3}x_0$ for the example of a 1 kHz signal propagating in a saturated internal-wave field. Typical oceanographic scales for this example have been estimated from several sources [10–12] and used as input to the expressions given in figure 1. The parameter τ_0 represents the characteristic lifetime (temporal coherence scale) of the oceanographic inhomogeneities, and $\tau_a \approx \tau_0(\Gamma x/x_0)^{-1/2}$ represents the corresponding acoustic time scale. The results are displayed in table 1.

Note that the ribbon time coherence, τ_a , is generally less than the oceanographic time scale, τ_0 . This is true from an Eulerian perspective (where the receiver is fixed in space), the focused ribbon viewed from a Lagrangian frame (moving with the ribbon) would have $\tau_a \approx \tau_0$. The region of maximum random focusing for our internal-wave example occurs at

Table 1. Typical scale sizes for 1 kHz acoustic ribbons in an internal-wave field.

Acoustic field	Oceanography	Acoustic streamers
Frequency = 1 kHz	$L_h = 6$ km	$\xi = 3.9$ km
Sound speed = 1500 m s ⁻¹	$L_v = 150$ m	$\eta = 1.2$ km
		$\zeta = 30$ m
$\lambda = 1.50$ m	$\mu^2 = 5 \times 10^{-9}$	$\Gamma = 50$
$k = 4.19$ m ⁻¹	$\tau_0 = 4$ h	$\tau_a = 1$ h
		$x_f = 23$ km

**Figure 2.** Site of the experiment in the eastern Mediterranean.

some 23 km, clearly physically realizable in the ocean and of considerable relevance to sonar system performance. The sizes of the ribbons are about 2.5 km in the horizontal and 30 m in the vertical, smaller than the oceanographic scales (as expected), but certainly significant with respect to towed array apertures. At higher frequencies, the relevant oceanographic scales reduce as f^{-1} , while Γ , which is dimensionless, remains roughly constant.

The range for maximum focusing also behaves as f^{-1} . For frequencies $O(10^2)$ kHz, the relevant ocean variability scales would then become $O(10^0)$ m in the vertical, and rather larger in the horizontal. These scales are appropriate for turbulent fields caused by tidal or other rapid flows in near-shore and shallow waters. Providing sound-speed inhomogeneities were indeed present in sufficient strength at these spatial scales, the random focusing would be expected to become most significant over a range of $O(10^2)$ m, in the minehunting sonar range.

Since these scales are of obvious relevance to the operation of underwater acoustic systems, we decided to try to detect such ribbons in a qualitative ocean-acoustic experiment. To obtain a convenient data sampling rate and match available sources, we chose a frequency of 3.5 kHz and decided to look for focused ribbons in the 10–20 km range. We then required a deep-water site (to avoid surface and bottom interactions and allow us to separate individual ray-path arrivals) with known oceanographic variability. The site chosen was in the eastern Mediterranean (figure 2). Even if internal waves were found to be inactive, Wust [13] has shown that this

region contains a rich mixture of different water types that would hopefully provide abundant acoustic scattering inhomogeneities. There were therefore good prospects for observing a multiply scattered acoustic field with well developed ribbons at an appropriate frequency and range.

2. Experimental configuration

The crucial aspect of this experiment was to measure the acoustic field synoptically over a sufficient depth and range aperture with appropriate resolution. The apertures must be at least several times the acoustic ribbon horizontal and vertical scales in order to have some success in detecting whole ribbon features. At the same time, the vertical and horizontal resolution should be high enough to place several independent measurements within each ribbon. Finally, we required a source–receiver geometry and signal design for which multipaths could be separated, so that the random focusing could be examined in the absence of multipath interference effects. In addition, the total observational aperture needed to be several hundred metres deep and several kilometres long. There existed no equipment capable of acquiring acoustic data with such a vertical and horizontal resolution over such an aperture. The nearest approach we could implement was to use a 32 hydrophone vertical array, of 62 m aperture and 2 m resolution, in a ‘yo-yo’ mode from a drifting ship.

The idea was to raise and lower the array in steps of 62 m to synthesize a total vertical aperture of over 100 m, while the ship drifted away from a moored source to provide the horizontal aperture. Providing that the ship drifted at moderate speed (0.5 kt), we expected to cover perhaps 4 km horizontal aperture during one Lagrangian lifetime of the ribbons. At each array deployment, approximately 60 s of data were collected. The experimental arrangement and an example sound-speed profile (calculated from a CTD cast) are shown in figure 3. The RECMASS buoy is a self-contained source-deployment buoy that was moored to the sea floor.

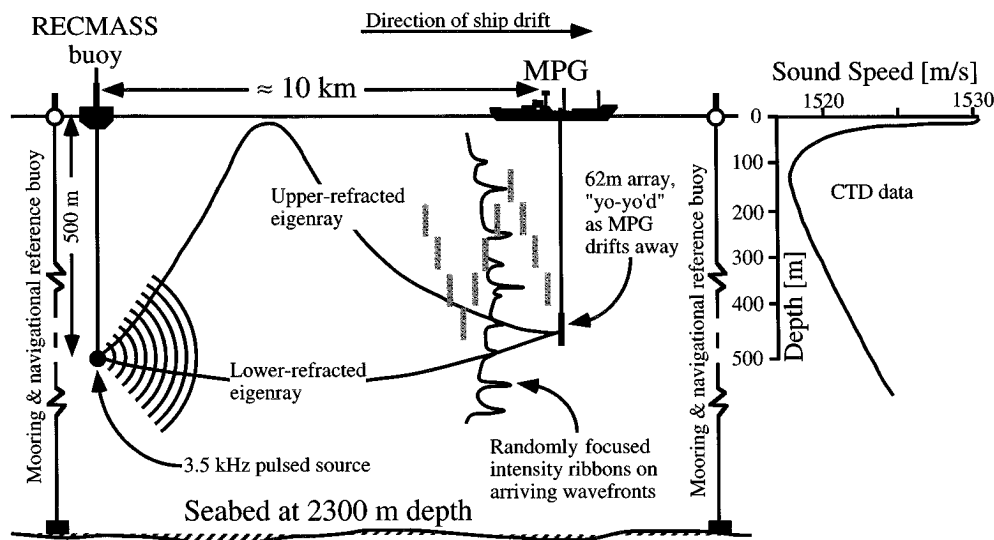


Figure 3. Experimental configuration of the moored source and ship-deployed receiver array. A typical sound-speed profile, taken during the course of the experiment, is shown on the right-hand side of the figure.

RECMASS has a signal generator and amplifier which drives a suspended source which was positioned at 500 m depth. Figure 3 shows that both the source and array depths were kept within a broad, deep sound channel. For this geometric configuration, there are two connecting rays that do not interact with the surface or bottom, one upper and one lower refracted. The geometry and sound-speed profile preclude any connecting surface reflected rays. In order to separate the two refracted rays, a 10 ms pulsed CW signal was transmitted at a centre frequency of 3.5 kHz at 5 s intervals. The signal was received at the research ship Maria Paolina G (MPG) and the signals gated in the time domain to separate arrivals. Each array position then yielded 12 independent estimates of signal intensity over the 60 s recording period.

3. Results

A preliminary account of this experiment was presented as part of a short article in the British Acoustics Bulletin in 1988 [14]. The environmental data had not been analysed at that time, and only an approximate idea of the acoustic intensities had been calculated. The complete experimental results are presented here in two parts, environmental and acoustic. The environmental results are given first and evaluated to provide a qualitative basis for understanding the acoustic impact of the oceanographic inhomogeneities.

3.1. Environmental results

A typical vertical sound-speed profile is shown in figure 3. Although the data extend to over 1600 m depth, only the upper 500 m are shown, since below this depth the profile shows only a uniform increase due to the pressure effect. The vertical array was deployed at depths ranging from 100 to 500 m, so that the source and receivers were always within the sound channel. Bottom reflections arrived much later than the lower and upper refracted pulses and were gated out in the time domain.

3.1.1. Towed oscillating body measurements. It was planned to carry out simultaneous towed oscillating body (TOB) casts from a supporting vessel along the propagation track. The TOB is a CTD package that can be towed through the water in a vertical 'zig-zag' track to provide a two-dimensional section of the water properties. Such sections can be used to separate internal wave from other variability effects and to characterize the horizontal and vertical scales of the inhomogeneities [11]. Unfortunately, the supporting vessel for this TOB deployment was able to conduct only one such cast, immediately before the acoustic data collection, before mechanical problems forced her to withdraw. We are thus unable to present simultaneous environmental data that can be quantitatively matched to the acoustic results. However, the one available cast does give an idea of the environment and an estimate of the proportion of inhomogeneities arising from internal-wave activity versus water-mass mixing. We shall therefore examine this one TOB cast for the circumstantial information that it can supply.

The maximum TOB tow depth was 240 m. The single section obtained by the environmental support vessel was taken on a heading of 90° T for a distance of 3 km, followed by a course of 14° T for a further 9 km. From this cast, a two-dimensional section of the sound-speed structure can be estimated, from which it was immediately apparent that the sound-speed field was far from horizontally homogeneous. Let us define a residual field to be the result of subtracting the range-averaged value from the field at each depth. A residual field shows the anomaly of the field with respect to the mean vertical profile. The residual sound-speed field (interpolated so as to respect a 50:1 horizontal:vertical scale ratio in the

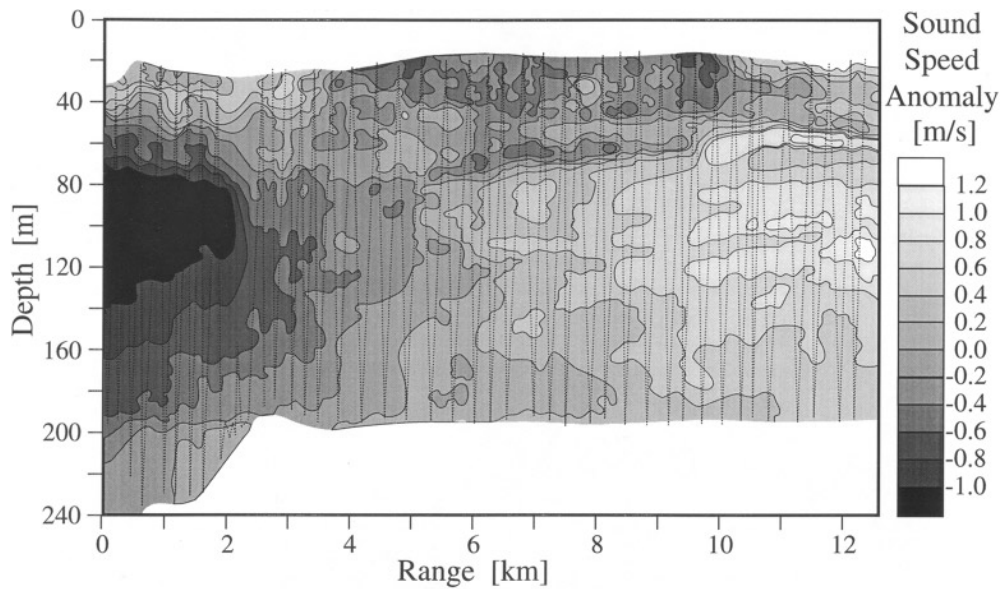


Figure 4. Residual sound-speed anomaly, calculated from the TOB cast.

ocean) is shown in figure 4, where the zig-zag path of the TOB is shown by the dotted line. Clearly the predominant variability occurs on a large scale (compared to the cast length) with a large ($\sim 2.5 \text{ m s}^{-1}$) difference in sound speed from the beginning to the end of the cast at 100 m depth.

To understand the origin of this sound-speed anomaly field, we need to look at the residual fields of salinity and potential temperature displayed in figures 5(a) and (b). These figures illustrate that there is a relatively cool and fresh water mass found at the beginning of the cast, contrasting with warm and salty water at the end. The almost perfect correlation between the potential temperature and salinity residual fields confirms that the inhomogeneities are generated by linear mixing between two primary water types rather than by internal-wave activity. The residual potential density field (not shown) confirms this interpretation, and shows that the frontal boundary could not have been in static equilibrium, since there is a mean potential density gradient of some $10 \text{ kg m}^{-3} \text{ km}^{-1}$ at 100 m depth. This gradient may have been partially balanced by a geostrophic current.

3.1.2. Wave and non-wave separation of ocean inhomogeneities. Two-dimensional sections of potential temperature, salinity and density allow the separation of wave and non-wave components of the inhomogeneities in the sound-speed field [11]. For this TOB cast, the low-wavenumber results will be somewhat distorted due to the curved path of the TOB track, but the high-wavenumber results are little affected and the overall results were still clear.

The separated wave component was compared with the internal-wave model of Munk and Zachariasen [10] with f_0 (the buoyancy frequency) and B (the vertical $1/e$ buoyancy scale) calculated from the observed Brunt–Vaisala profile to be 9 cycles/h and 250 m, respectively. There is a strong trend for wave energy levels to decrease with depth for all wavenumbers in the experimental observations, as one would expect in an internal-wave field. The spectral slope is nearly $\beta^{-3/2}$ (where β is the horizontal wavenumber) for depths below 100 m in good agreement with internal-wave theory. Shallow data show only a weak wavenumber

dependence, suggesting that surface processes dominated these results. The refractive index variance at the deepest observations due to internal waves was determined to be approximately 3×10^{-9} , and this energy was chosen as a free parameter to fit the internal-wave model to the data.

The corresponding non-wave field for the same data displays a very different spectral slope because, as might be expected, these spectra have a turbulence-like slope near $\beta^{-5/2}$ rather than $\beta^{-3/2}$ as for internal waves. There is also very little depth dependence of the non-wave field energy. Finally, the overall inhomogeneity strengths are much higher, by a factor of four or more, compared to the wave component. These are encouraging results, confirming the expectation that the sound-speed inhomogeneities are dominated by frontal-like mixing processes rather than internal waves. The spectral slopes, depth dependence and overall energy partition between the wave and non-wave fields are consistent with expectations for such processes.

3.1.3. Environmental length scales. We would like to estimate length scales for the residual sound-speed field for input to the multiple-scattering theory. Unfortunately, there is a strong horizontal length-scale component of 10 km or more which obscures the smaller scales. We are therefore not in a position to evaluate L_h and L_v *a priori* solely from the environmental data. We can, however, state certain restrictions on the values that these parameters may take, given that we do observe random focusing in the 10–20 km range (as we shall see). These bounds are as follows.

- (a) Horizontal inhomogeneity scales of $O(10^1)$ km will not contribute to random focusing at ranges of 10–20 km, but will (to first order) only impart a smoothly varying phase modulation on the wavefront at that range. The scales that will cause random focusing must be smaller. Such features do exist in the TOB cast, but are obscured by the more energetic larger scales, since the intensity decays rapidly with horizontal wavenumber (as $\beta^{-5/2}$). We conclude that for those inhomogeneities that give rise to random focusing in the ranges of interest, $L_h < 5$ km.
- (b) Let the ratio of horizontal to vertical scales in the ocean, $\alpha = L_h/L_v$. We expect α to lie in the range 10–200, these values being the limits of similar prior observations [10–12]. As an aside, we do not expect α to be strongly dependent on the absolute values of L_h and L_v . This is equivalent to assuming that the inhomogeneities are self-similar over the relevant scale range. Self-similarity over a range of scales is frequently found in turbulence and mixing problems. We have already confirmed that our inhomogeneities are indeed driven by mixing rather than internal waves.
- (c) The multiple-scattering parameter, $\Gamma = k^3 \mu^2 L_h L_v^2 \gg 1$ for random focusing to occur [9]. We begin by estimating μ^2 for the two paths (lower refracted and upper refracted). Note that μ^2 is very nearly equal to the value of refractive index variance, and so they can be used interchangeably. The value of μ^2 has been calculated as a function of depth from the TOB data, after mean and trend correction. Values above 100 m have not been evaluated as the TOB path ceases to provide sufficient horizontal resolution above this depth. This is not a severe limitation, since no connecting ray travels in this upper 100 m for more than a 2 km distance ($< L_h$) so the value of μ^2 in this region contributes little to the multiple scattering. Values of μ^2 below 240 m are not available, due to the depth constraints on the TOB. Note also that the values between 200 and 240 m may be unrepresentative since only a few TOB data cycles were obtained at these depths. We shall assume that the value of μ^2 remains approximately constant at depths over 200 m. We take this to be the most reasonable assumption, given that we know the ocean inhomogeneities to be driven

Table 2. Anticipated ribbon scale sizes at 13 and 21 km for lower and upper rays.

	Lower ray		Upper ray	
	13 km range	21 km range	13 km range	21 km range
μ^2	5×10^{-9}	5×10^{-9}	1×10^{-8}	1×10^{-8}
L_v	200 m	200 m	180 m	180 m
L_h	4 km	4 km	3.6 km	3.6 km
Γ	2400	2400	3500	3500
x_f	39 km	39 km	28 km	28 km
ζ	19 m	15 m	13 m	10 m
η	280 m	300 m	260 m	200 m
ξ	5.3 km	3.3 km	2.4 km	1.5 km

by mixing and to be only weakly depth dependent at distances sufficiently far from the surface. The value of μ^2 for each connecting ray should be a path integral of the values encountered along the ray path. For the lower ray, we therefore set $\mu^2 = 5 \times 10^{-9}$, the assumed constant value below 200 m. For the upper ray, we set $\mu^2 = 1 \times 10^{-8}$, twice the lower connecting ray value to allow approximately for the passage of these rays through the very active region above 200 m depth.

We now proceed to assign values to the environmental scale parameters for the two connecting rays. We choose $\alpha = 20$ in accordance with the anisotropy of layer features in equilibrium in the ocean. For the lower ray, we set $L_v = 200$ m, so that $L_h = 4$ km, which is consistent with the single available TOB cast and the above restrictions. For the upper ray, we assume that the scales will be rather smaller, though the evidence is that the difference is only slight. We therefore set $L_v = 180$ m, and hence $L_h = 3.6$ km. We may now calculate the multiple-scattering parameters relevant to acoustic ranges of 13 and 21 km (chosen to coincide with the mid-points of the two experimental acoustic runs) for the upper and lower refracted rays. Table 2 gives a guide to the expected ribbon scales and confirms that there are sets of inhomogeneity scales and strengths consistent with our environmental observations that are expected to result in observable multiple-scattered random focusing at 13 and 21 km.

3.2. Acoustic results

Two sets of yo-yo drift data were taken, providing two ‘snapshots’ of the ribbon field over different depth and range apertures. These results will be referred to as ‘run 1’ and ‘run 2’. Before presenting these data, we briefly describe the data reduction and analysis procedures developed to extract the signal amplitudes of individual arrivals.

3.2.1. Data reduction and analysis. The only significant change in experimental set-up between runs 1 and 2 was that run 2 was taken at a greater range and over a more limited depth range than run 1. The data analysis procedure for the two runs was identical. The data were sampled at 12 kHz and a pass-band filter of width 250 Hz (at the -6 dB points) was used to select the pulses. To reduce mass storage requirements the data were then sub-sampled at 2 kHz, beating the observed carrier frequency down to 500 Hz, and recorded. The band-pass filtering and subsampling caused the sharp rise and fall of the pulse envelope to become smeared, increasing the effective pulse length from 10 to 13 ms. Each recording at a fixed depth lasted 60 s, in which some 12 pulsed signals would arrive, then the array would be raised or lowered, and a few minutes later another record taken.

The signal-to-noise ratio (SNR) was high (some 25 dB). For well separated arrivals, a simple matched filter was sufficient to estimate the amplitude. The well resolved pulses do not display significant inter-pulse variability (other than amplitude), indicating that pulse distortion can be neglected. Where pulse arrivals from the two eigenpaths overlapped, a more sophisticated signal-processing technique was required. Since the two arrivals overlap with an unknown relative phase, a quadrature matched filter correlator was applied using a set of matched filters. Each matched filter consisted of a simulated complex exponential two-arrival pulse with the relative carrier phase difference, amplitude ratio and relative lag chosen as free parameters. The modulus of the correlator output was normalized by the integrated matched filter power and used as a cost function which was globally optimized. This was repeated for all 12 signals obtained in each recording. Outlying estimates among the 12 realizations were discarded until the number of acceptable estimates became too small, or the inter-estimate variance fell below a threshold. By means of this algorithm, satisfactory results were obtained for pulses that were separated by as little as 4 ms, verified by using simulated data with representative white noise. At less than 4 ms separation, sidelobe suppression in the likelihood surface degenerated sufficiently to incur aliasing errors.

We can compare this 4 ms performance limit with the Cramer Rao lower bound (CRLB) calculated for this problem. Ianniello and Hamilton [15] give an expression for the CRLB in the case of estimating the arrival time of a single signal at one receiver. The value of $(\text{CRLB})^{1/2}$, which gives the minimum RMS expected error of an unbiased estimator, is 1.5 ms for this case, using our values of the bandwidth, SNR and pulse length. Our problem is slightly different, in that we wish to estimate the arrival time of a second signal in the presence of the first, which overlaps it. This is akin to estimating the arrival time of one signal in the presence of increased noise (the other signal). If we take $\text{SNR} = 1$ to allow for the effects of the overlapping neighbouring pulse, then $(\text{CRLB})^{1/2} = 8.4$ ms. The total error in estimating the difference in arrival times would be greater by $\sqrt{2}$ (the joint error expectation if the errors are uncorrelated) and less by $\sqrt{12}$ (the number of independent estimates), giving a final minimum expected error of 3.4 ms. This is consistent with our results.

In addition, Ianniello and Hamilton have pointed out that the thresholding effect ensures that the CRLB performance is unattainable except in the limit of high SNR and high time bandwidth. Although our SNR is large, the time bandwidth is about 1—as low as it can get. The thresholding behaviour has the effect of degrading the estimator performance rapidly, rather than smoothly, once the threshold is exceeded. This is precisely the nature of the effect we observe of aliasing onto neighbouring sidelobes of the ambiguity surface. We conclude that our estimator is threshold-constrained and that it has near-optimal performance for the signal-processing conditions.

The range at each recording segment was calculated from navigational data obtained from recorded radar ranges to the RECMASS and a navigational reference buoy. Once all the data for a run had been assembled, the values were interpolated into a regular grid with grid cells of dimension 1 m in the vertical and 50 m in the horizontal direction, as for the environmental data. The grid-cell shape respects the natural scaling of the ribbons during the nearest-neighbour search algorithm of the interpolation. It is also based on the anisotropy inherent in an acoustic field in which the component plane waves propagate at very small angles with respect to the forward direction. This is an important characteristic of such fields, of which the present one is an example. It is discussed in the appendix. However, all interpolated results presented in this report show the true position of the hydrophones, or ground-truth data points, so that the reader can assess for himself the extent of interpolation artefacts.

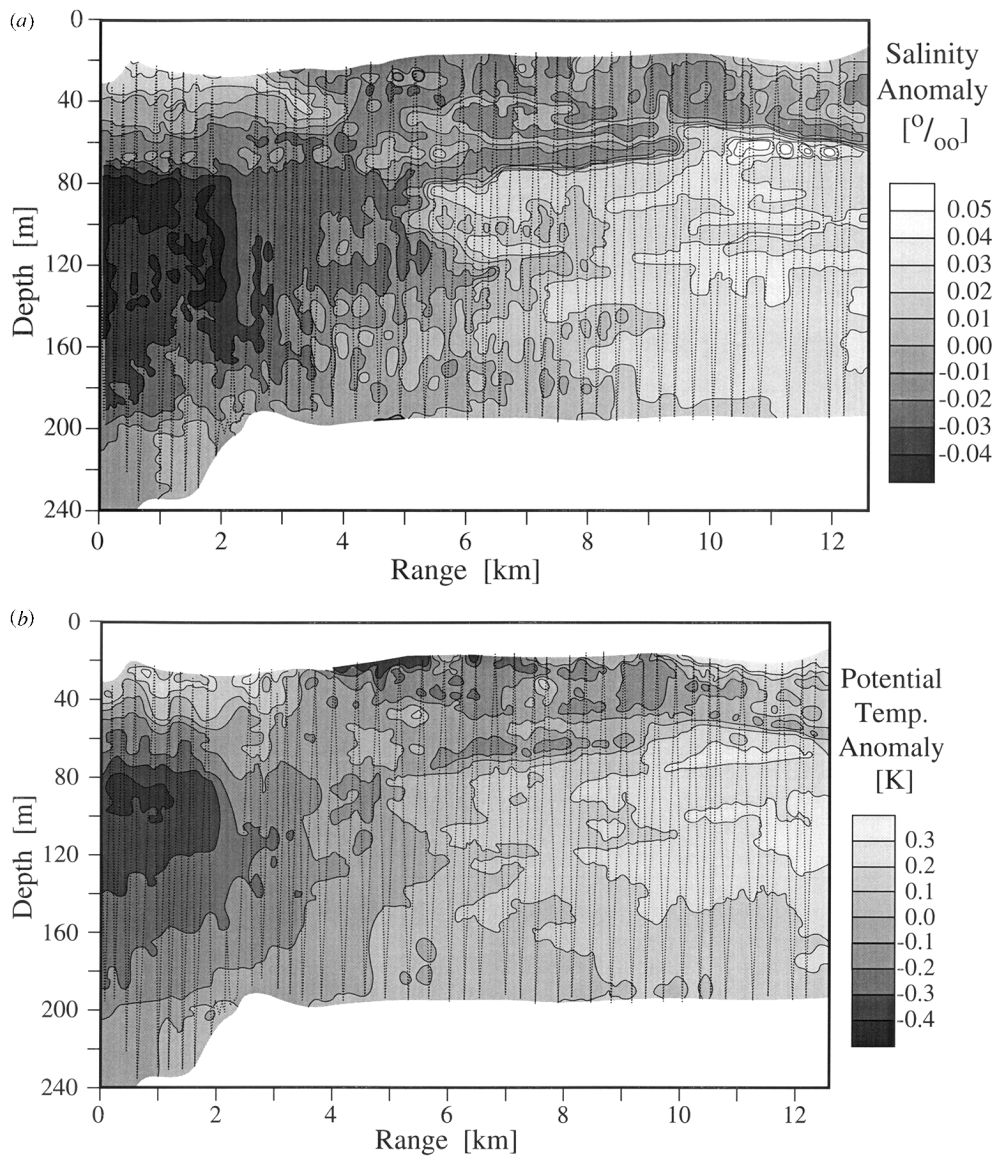


Figure 5. (a) TOB cast of residual salinity anomaly. (b) Corresponding residual potential temperature anomaly.

3.2.2. The first acoustic run. Run 1 was taken at a starting range of 10.9 km on 21 June 1986. The vertical array was yo-yo'd from the surface to 510 m depth for three cycles. A total of 42 recordings were made over a period of 328 min, during which the ship drifted 4 km. For data collected at depths less than 110 m, resolving the two arrivals became unreliable. The near-surface recordings have therefore been disregarded, as have three at maximum depth during the run. The remaining 33 recordings span a range of 3.9 km at depths from 120–460 m over a time period of 305 min.

Clearly there will be some time contamination of the spatial results. The Lagrangian

lifetime of a ribbon is expected to be approximately that of the generating inhomogeneities. It is difficult to estimate the temporal inhomogeneity coherence, but mixing features such as those in figure 5 typically persist for days rather than hours. Since a single ribbon will be traversed in an hour or less (table 2) we do not anticipate significant temporal–spatial contamination. A more serious concern is whether the ship's drift rate provides suitable horizontal resolution. The effective resolution varies, due to the yo-yo path, but averages some 600 m. The drift track was not along the line of propagation, but at approximately 35° to it. The expected horizontal ribbon scale is therefore about 1.3 km. The horizontal resolution is therefore just sufficient to resolve the expected ribbons. Finally, the vertical and horizontal apertures of 340 m and 4 km, respectively, should be sufficient to capture whole ribbons.

The intensity was separately predicted with a standard propagation model for each of the two eigenrays. As expected, the results show a smoothly varying and nearly depth-independent value for each ray, whose amplitude decreases smoothly and monotonically by some 2.5 dB over the range aperture due to spreading losses. The amplitude predictions for both rays are similar and show no complex structure.

The data were processed to estimate the signal intensity arising from each of the two eigenrays separately. The observed amplitudes are displayed in figure 6 for the upper (*a*) and lower (*b*) refracted rays, normalized to an arbitrary dB level to display the anomalies. The positions of the hydrophones in the array are marked by dots, but they are so close together on this scale that each array position appears as a full vertical line. The vertical:horizontal scaling of the plots is in the ratio 10:1 because of the inherent anisotropy of the acoustic field as explained in the appendix, and the dynamic range has been chosen to enable the results from both runs to be displayed on the same colour scale.

The procedure used to construct the intensity contours of figures 6 and 7 needs to be explained at this stage. The intensity was measured where shown by the small dots. The acoustic intensity can vary only slowly in the horizontal direction because of the inherent anisotropy of the sound field as shown in the appendix. This imposes a quantitative condition on the manner in which the measured acoustic intensity can be extrapolated in the horizontal direction.

In the vertical direction the acoustic intensity pattern observed along each array length can be extrapolated both upwards and downwards beyond the array. Since successive array positions are staggered, i.e. each vertical position is further advanced in the horizontal direction relative to the previous position, this vertical extrapolation provides extra information before and after each array profile. It therefore imposes an additional condition on the horizontal extrapolation.

As a result of these two conditions the array observations can be extrapolated over a band on either side of the array positions. In between the bands the values are interpolated on the basis of two conditions. The first of these is the inherent anisotropy of the acoustic field and the second is that of a smooth connection with the extrapolation bands.

The intensity contours inside the interpolation areas are subject to a degree of uncertainty but the process is biased to smoothing out and removing features rather than creating them. These interpolation areas are denoted in figures 6 and 7 by horizontal wavy lines.

We see that many of the important features in the acoustic intensity contour maps are fairly well covered by the more certain extrapolation areas. At the same time there is quite a reasonable indication that these features are rather extended in the direction of propagation, i.e. the observations are consistent with the predictions of long ribbon-like structures.

The only similarity between the observations and the deterministic prediction is the weak trend of decreasing intensity with range. The lower refracted ray displays some relatively

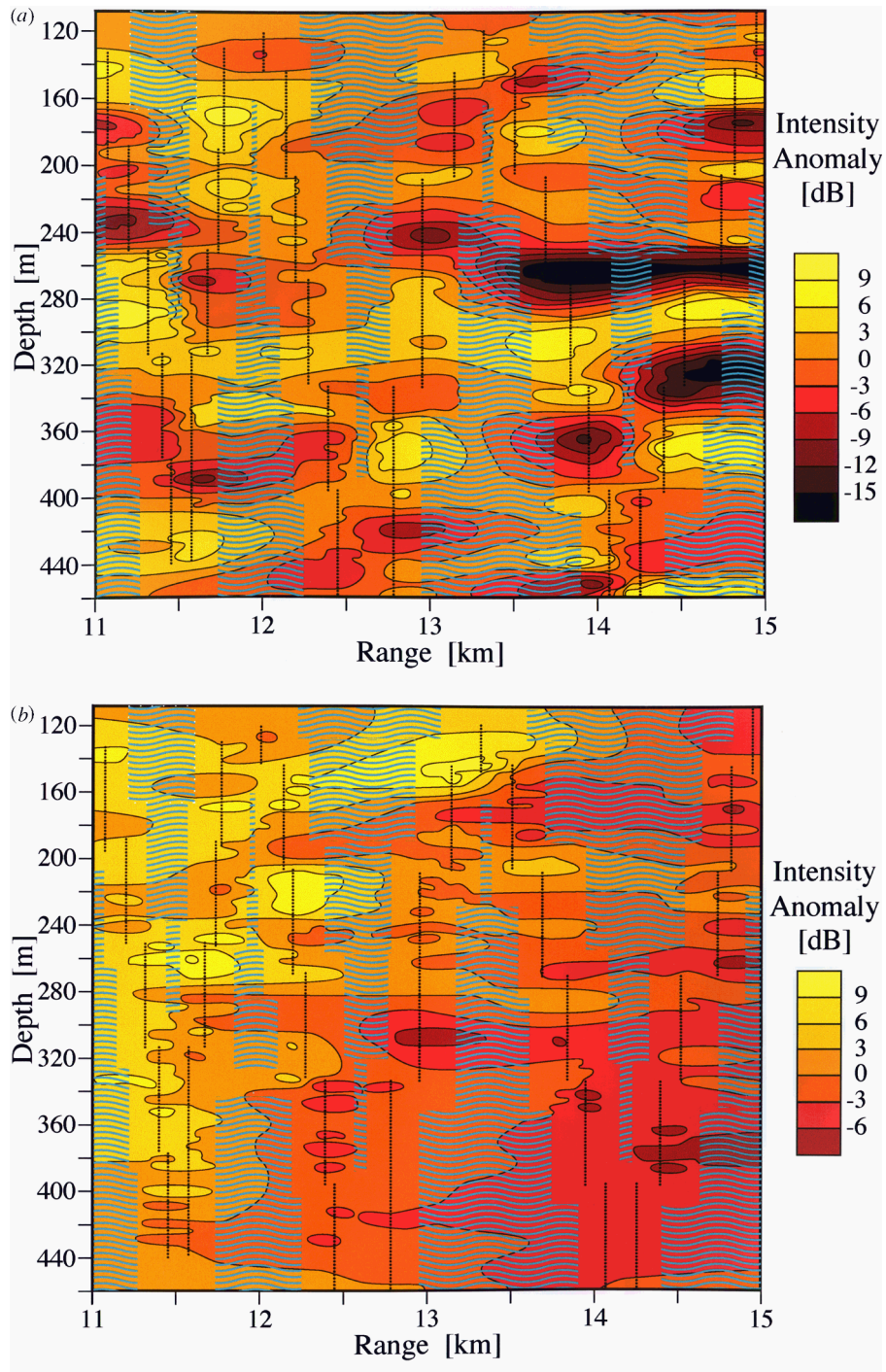


Figure 6. Acoustic intensity for the upper (a) and lower (b) refracted ray path from run 1.

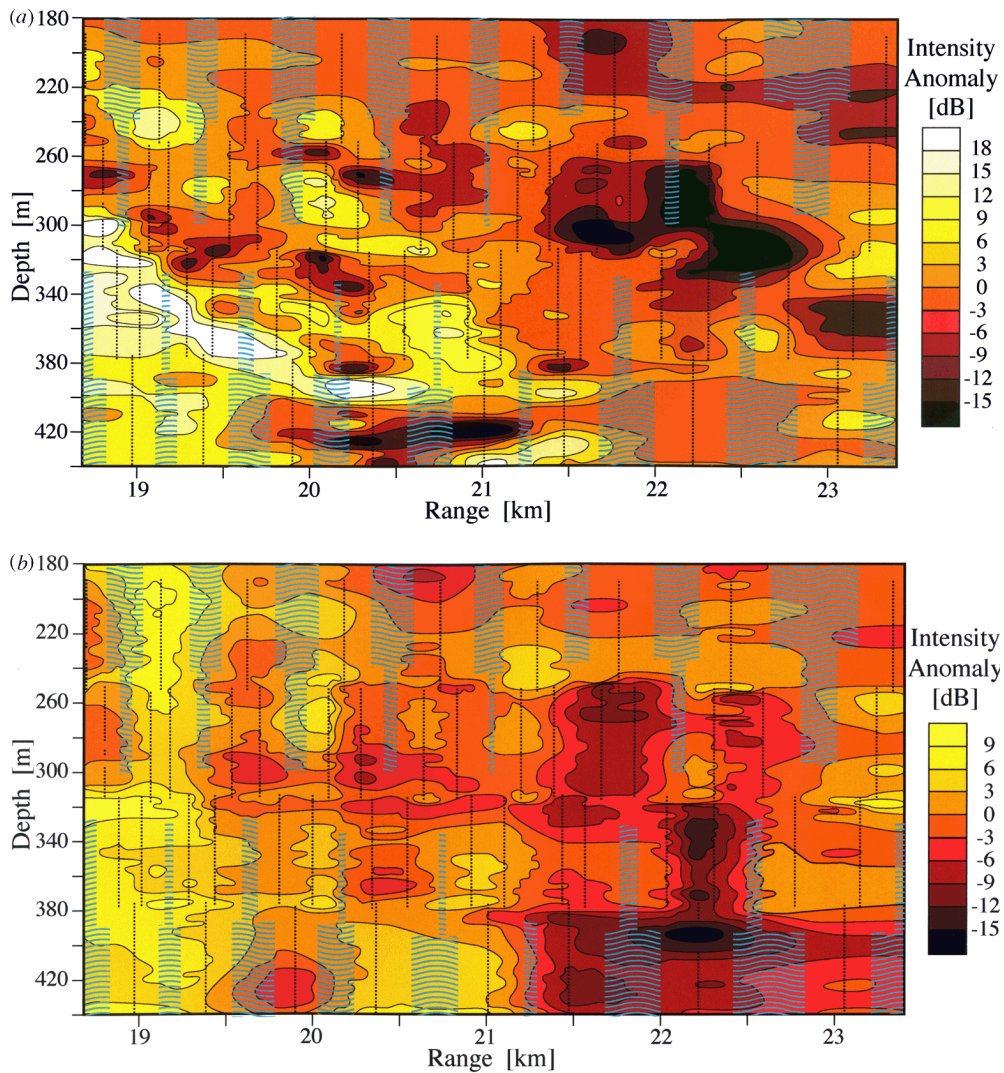


Figure 7. Acoustic intensity for the upper (a) and lower (b) refracted ray path from run 2.

weak ribbons of about 4 dB strength. The upper refracted ray, shown on the same dynamic range for comparison, displays more numerous, stronger ribbons of typically 9 dB. The ribbon patterns for the two rays are uncorrelated, as one would expect from an effect caused purely by vertically refracted path histories separated by more than L_v . We emphasize that these two maps are of ribbons that co-existed in space and time. The ribbons are not physical entities, but high-amplitude regions associated with a single connecting ray.

The observed ribbons for both ray paths appear to have similar scales, some 1–2 km long and 20 m deep. If there is a difference in the vertical scales, the upper ray generates thinner ribbons. The horizontal scale has little meaning because the sparsity of the horizontal resolution prevents anything more than a sketchy idea of the true ribbon shapes. The vertical

resolution (2 m) and aperture (62 m) at least guarantees the vertical coherence of the ribbons has been adequately resolved, and is not an interpolation artefact. The similarity of vertical scales for the two rays implies that the environmental inhomogeneities encountered along the upper-refracted ray were indeed of similar or slightly smaller vertical scale to those encountered by the lower-refracted ray. This justifies an assumption we made in creating table 2. The ribbon dimensions appear to be slightly larger in the vertical direction than predicted in table 2 but the difference is of questionable significance, considering that we do not have synoptic oceanographic data along the transmission track.

The strengths of the ribbons due to the two paths differ by some 5 dB, the near-surface ray causing the stronger focusing. This is expected from the decrease in refractive index variance and slight increase in vertical scale with depth; rays that pass nearer the surface experience stronger scattering by slightly smaller features. Table 2 indicates that the expected region of maximum random focusing, x_f , is some 28 km for the upper ray, compared to 39 km for the lower one. The mean observation range of 13 km then corresponds to a point nearer the peak focusing for the upper ray, with a concomitant increase in the ribbon strength and a slight decrease of the vertical ribbon scale, as observed.

The most impressive feature in figure 6 is an acute null in the acoustic field between 13.7 and 14.7 km range at 260 m depth for the upper ray path. This might be dismissed as an instrumental or data-processing error except that it is clearly observed on two consecutive deployments of the array at that depth and does not appear on the lower ray path acoustic results. The field intensity in this null is some 20 dB below the mean.

3.2.3. The second acoustic run. Run 2 was started the following day, using largely the same procedure as for the first. The array was yo-yo'd over a smaller depth range, giving a reduced vertical aperture but improving the horizontal resolution. In addition, the run was started at a greater range from the source, 18.7 km. The 49 recordings selected for analysis comprise eight yo-yo cycles taken over a period of 309 min and spanning a range of 4.6 km over depths of 190–440 m. The horizontal resolution averages 290 m, in contrast to 600 m for the first run.

As for the first run, the predicted unscattered intensity decreases monotonically by some 2 dB due to spreading losses over the observed range. The observed amplitudes are displayed in figure 7 for the upper (*a*) and lower (*b*) refracted rays, again normalized to an arbitrary dB level. The array positions are marked by vertical lines. The vertical and horizontal scaling of the plots, as well as the dynamic range, have been kept the same as for figure 6 so that a direct comparison is possible. The lower refracted ray displays some ribbons of typically 6 dB, slightly stronger than for the lower ray of run 1. The upper refracted ray, shown on the same dynamic range for comparison, displays many, stronger ribbons of typically 15 dB and sometimes in excess of 21 dB. Once again, the ribbon positions for the two rays are uncorrelated, as expected.

The ribbons observed in the second run differ substantially from the first run in strength, which is some 2 dB higher for the lower refracted ray and 6 dB higher for the upper refracted one. In addition, the scales appear to be somewhat smaller for the second run, though this may be partially due to the increased detail revealed by the stronger anomalies. These effects are consistent with the predictions of table 2. As one increases the observation range from the near-field region to the peak focusing range, the size of the ribbons become somewhat smaller (as $\text{range}^{-1/2}$) and the strength of the intensity anomalies increases rapidly. There is also at least one severe low-intensity (null) ribbon.

4. Conclusions

A conceptually simple, but logistically difficult, experiment has been conducted to investigate an interesting prediction of multiple-scattering theory. The experiment would not have been possible if the sea had not been particularly smooth and the ship's drift rate suitably gentle (<0.5 kt). It is unfortunate that the planned full environmental data collection could not be carried out to provide a quantitative test. Despite this limitation the trial yielded some important information about the spatial structure of multiply scattered sound in the ocean. First, the extent of the vertical aperture over which the acoustic intensity was observed (250–350 m) was appreciably greater than any previous trial, and showed clearly that focusing into narrow features with vertical dimensions of the order of 20 m takes place, and that contrasts of 6–18 dB can occur.

Secondly, the fact that these 'vertical' profiles were staggered allowed use to be made of physical constraints to produce two-dimensional contour plots of the acoustic features. These contour plots reveal elongated or 'ribbon'-like features that are consistent with theoretical predictions based on available oceanographic data. The random focusing effect can easily be of the order of 12 dB and sometimes exceeded 20 dB, for realizable frequencies and scales relevant to operational sonars. The intensity fluctuations are observed at neighbouring hydrophones, and occur at different places along the array at each recording. This indicates that the fluctuations we observe are not instrumental artefacts, but physical effects present in the ocean. The vertical scales of these fluctuations have been resolved, but the horizontal scales we estimate may be somewhat in error due to the sparse sampling of the yo-yo method.

Theory tells us that such ribbons will occur at appropriate ranges at any frequency, provided there are scattering inhomogeneities of an appropriate size and sufficient strength. The ocean contains significant scattering features at all scales from turbulence to open-ocean eddies (10^{-2} – 10^5 m), which will multiply scatter frequencies of the order of 10 MHz down to a few tens of Hz. The resulting random focusing will occur at ranges of less than 1 m, in the case of fine-scale turbulence, to perhaps 10^6 m, in the case of VLF mega-metre transmissions as used for monitoring global warming. As the use of ocean acoustics is increasingly extended into remote sensing applications, the impact of random focusing due to multiple weak scattering will become an increasingly important issue in system performance and optimization.

Acknowledgments

We wish to gratefully acknowledge the willing and most hospitable support of the Turkish naval forces in the execution of this experiment. The authors are also pleased to be able to thank the many 'unsung heroes' in the support groups at Saclant Centre who designed, built, prepared and deployed equipment with unstinting technical support.

Appendix

An important characteristic of the acoustic field that helps in interpreting the data is its inherent anisotropy. The scattered field associated with a particular eigenray can be considered as consisting of a set, or spectrum, of plane waves propagating at small angles with respect to the ray, i.e. in the 'forward' direction.

Let (x, z) be a set of Cartesian axes with the x -axis in the 'forward' direction. Consider

a single plane wave propagating at an angle θ to the x -direction. It can be written as

$$E(x, z) = A(s) \exp\{ik[Sz + Cx]\} \quad (\text{A1})$$

where

$$S = \sin \theta \quad C = \cos \theta \quad (\text{A2})$$

and $A(s)$ is the amplitude and k the wavenumber. Since θ is a small angle this can be written as

$$E(x, z) = A(s) \exp\{ikx\} \exp\{ik[Sz - \frac{1}{2}S^2x]\}. \quad (\text{A3})$$

The spatial periods of the components in the z and x directions are, respectively,

$$z_0 = \lambda/S \quad x_0 = 2\lambda/S^2. \quad (\text{A4})$$

The ratio of these spatial periods is

$$x_0/z_0 = 2/S \quad (\text{A5})$$

which, since S is small, is elongated in the x -direction. An acoustic field that consists of a set of such plane-wave components will also exhibit the same anisotropy in its spatial structure.

We now estimate the degree of spatial anisotropy to be expected in the present experiment. Simple diffraction theory suggests that S , the angle of scatter of the acoustic field, is given by

$$S \approx \lambda/\zeta_0 \quad (\text{A6})$$

where ζ_0 is the vertical scale of the feature in the observed intensity pattern and λ is the acoustic wavelength. In the present case ζ_0 is of the order of 20 m and λ at 3.5 kHz is 0.43 m. Thus the degree of anisotropy to be expected in the intensity pattern is

$$x_0/z_0 \approx 2\zeta_0/\lambda \approx 90. \quad (\text{A7})$$

In view of the above a ratio of 50:1 was chosen for the horizontal and vertical sides of the cell when plotting the acoustic data.

Finally, the inherent anisotropy of the acoustic intensity patterns imposes a constraint on dI/dx , the rate of change of intensity in the x -direction that can occur when interpolating the acoustic data. The result (A7) would indicate that in the absence of other effects the upper limit of dI/dx should be of the order of $\frac{1}{90}$. However, it was decided to adopt a much less rigid constraint since additional scattering by the medium could increase this rate of change. An upper limit of the order of $\frac{1}{10}$ was chosen for dI/dx to reflect the inherent anisotropy of the acoustic intensity patterns while still allowing for the further effect of the medium.

References

- [1] Uscinski B J 1982 Intensity fluctuations in a multiple scattering medium. Solution of the fourth moment equation *Proc. R. Soc. A* **380** 137–69
- [2] Uscinski B J 1980 Parabolic moment equations and acoustic propagation through internal waves *Proc. R. Soc. A* **372** 117–48
- [3] Ewart T E 1989 A model of the intensity probability distribution for wave propagation in random media *J. Acoust. Soc. Am.* **86** 1490–8
- [4] Farmer D M and Crawford G B 1991 Remote sensing of ocean flows by spatial filtering of acoustic scintillations: observations *J. Acoust. Soc. Am.* **90** 1582–91
- [5] DiIorio D and Farmer D M 1994 Path-averaged turbulent dissipation measurements using high-frequency acoustical scintillation analysis *J. Acoust. Soc. Am.* **96** 1056–69
- [6] Macaskill C and Ewart T E 1984 *IMA J. Appl. Math.* **33** 1

- [7] Uscinski B J 1989 Numerical simulations and moments of the field from a point source in a random medium *J. Mod. Opt.* **36** 1631–43
- [8] Joia A 1993 Electromagnetic propagation through controlled turbulence *PhD Dissertation* Cambridge University
- [9] Uscinski B J 1986 Range and time dependence of acoustic intensity fluctuations *Ocean Seismo-Acoustics (NATO Conf. Series, Series IV: Marine Sciences)* ed T Akal and J M Berkson, vol 16 pp 253–67
- [10] Munk W H and Zachariassen F 1976 Sound propagation through a fluctuating stratified ocean: theory and observation *J. Acoust. Soc. Am.* **59** 818–38
- [11] Potter J R 1991 Finestructure in NAPOLI 85, an ocean/acoustic experiment *J. Acoust. Soc. Am.* **89** 1643–55
- [12] Cairns J L 1980 Variability in the Gulf of Cadiz: internal waves and globs *J. Phys. Oceanogr.* **10** 579–95
- [13] Wust G 1961 On the vertical circulation of the Mediterranean sea *J. Geophys. Res.* **66** 3261–71
- [14] Uscinski B J and Potter J R 1988 Sound ribbons in the sea *Acous. Bull.* **13** 24–8
- [15] Ianniello J P and Hamilton M 1989 Fundamental limitations to broadband time delay resolution for two sensors *IEEE Signal Process.* **37** 2661–4